Fusion Engineering and Design 148 (2019) 111261

Contents lists available at ScienceDirect

Fusion Engineering and Design

journal homepage: www.elsevier.com/locate/fusengdes

The properties of the tungsten coating on fine grain graphite using pulsed laser deposition

G. Antar[a,*], J. Ali[b], C. Madi[a], M. Noun[c], V. Rohde[d], M. Roumié[c], A.J. Said[b], J. Younes[a]

[a] American University of Beirut, Riad el-Solh, Beirut 1107-2020, Lebanon
[b] Lebanese University Section II, Fanar, Lebanon
[c] Lebanese Atomic Energy Commission-CNRS, P.O. Box 11-8281, Riad El Solh, 107 2260 Beirut, Lebanon
[d] Max-Planck Institut, IPP Garching, Germany

ARTICLE INFO

2000 MSC:
41A05
41A10
65D05
65D17

Keywords:
Tungsten coating
Carbon fiber composite (CFC)
ITER-like wall
Pulsed laser deposition

ABSTRACT

The advantages of using a high-*Z* material as a plasma facing component (PFC) in fusion devices is now admitted, consequently, the International Thermonuclear Experimental Reactor (ITER) will have a solid tungsten divertor. In this article, we present the properties of tungsten coating on fine grain graphite using the pulsed laser deposition (PLD) technique. We successfully achieve a uniform coating without cracks nor gaps while maintaining a low level of oxygen impurities in the deposited layer of about 1%. The coating shows tensile stresses as the body centered cubic (BCC) crystal structure of tungsten adapts to the graphite hexagonal structure. We use the Williamson-Hall method to distinguish the contributions of crystallite size and strain on the broadening of the X-ray diffraction peaks; The former increases from 30 to 50 nm while the latter saturates around 2.5×10^{-3} with increasing PLD laser energy. The Rutherford backscattering spectrometry (RBS) analyses show that the coating thickness is about 120 nm for PLD laser energy below 500 mJ. Around this value, the thickness increases abruptly to 300 nm and remains almost unchanged up to 600 mJ.

1. Introduction

Plasma facing components (PFC) in tokamaks and other magnetic fusion devices are crucial to their operation and lifetime. The sputtering of the PFC's generates impurities that pollute the core plasma and limit their space of operation. PFC's must be able to withstand high heat fluxes, reaching 10 MW/m^2, over a rather short period of time caused by edge localized modes (ELMs). These difficult problems led to many research experiments and investigations with the main goal to limit and control the influx of impurities into the core plasma as well as to lower the tritium retention in future devices. This is done by an adequate choice of the PFC material(s). Early usage of high-*Z* materials, like tungsten (W), on the PLT discussed by Hinnov et al. [1], or on TEXTOR shown in Sergienko et al. [2] led to rather disappointing results caused by the core contamination. Consequently, low-*Z* materials, mainly carbon-based PFC were later used by the various tokamaks worldwide. However, carbon has its own weaknesses, mainly its high physical as well as chemical sputtering yields. For this reason, the ASDEX-Upgrade group decided to return toward a full tungsten inner wall by coating the various components in steps before reaching 100% first tungsten wall. The results were presented by Krieger et al. [3], Mayer et al. [4], Herrmann et al. [5] and Neu et al. [6]. The difference between TEXTOR or PLT and ASDEX is the magnetic topography. A limiter has high temperatures that could go beyond the sputter threshold for W, while for divertor devices the low temperature allows only impurities as oxygen to sputter W. Moreover, the divertor retention reduces the W penetration into the core plasma. The different properties of the PFC's led to having ITER first wall composed of beryllium and tungsten as presented by Federici et al. [7] and by Philipps [8]. This brings another aspect to this problem discussed by Doerner [9] that is, mixed materials with the coating of one component the tiles made of other materials, hence, changing their properties.

Deposition of tungsten on graphite using electron beam evaporation, magnetron sputtering and arc deposition were compared by Maier et al. [10,11] with the goal to reach industrial-scale manufacturing. The first deposition type led to a high level of light impurities contamination, while the second suffered from low adhesion and the third one did not cover the same thickness range. Plasma assisted chemical vapor deposition (PACVD), done at the French association CEA-Euratom, produced tungsten films with thickness of 1–2 μm with a growth rate of 0.5 μm/h as reported by Cambe et al. [12]. Good adhesion on graphite was obtained but the samples presented oxygen contamination reaching

* Corresponding author.
E-mail address: ghassan.antar@aub.edu.lb (G. Antar).

https://doi.org/10.1016/j.fusengdes.2019.111261
Received 21 February 2019; Received in revised form 17 June 2019; Accepted 5 July 2019
Available online 02 September 2019

10%. Vacuum plasma spray of tungsten on graphite was performed by Liu et al. [13] and its thermal properties were studied as the coating was subject to a heat flux up to 5 MW/m^2. It was found that silicon could be considered as a good intermediate layer between the tungsten and the carbon. The 14 different samples with different coating types on CFC, namely CVD and PVD, and different thicknesses, presented delamination failure when subject to ELM-like heat loads as published by Maier et al. [14] and Neu et al. [6].

Ruset et al. [15] and Maier et al. [16] argued that the combination of magnetron sputtering and ion implantation (CMS-II) displayed high deposition rates of tungsten. A maximum thickness of 50 µm was produced. Problems concerning adhesion were solved by introducing a Molybdenum layer that decreased the global stress over the sample as discussed by Ruset et al. [17]. In the paper by Ruset et al. [18], it was found that the damage of the tungsten coating on CFC substrate occurred gradually with the increasing number of heat pulses. A dual process of atmospheric plasma spray and physical vapor deposition was investigated by Kim et al. [19] reaching a thickness of the multi-layered film over graphite about 100 µm. The presence of tungsten/molybdenum PVD deposited multilayer over the plasma sprayed tungsten prevented the intense microstructural change and surface erosion that would both occur in the case of simple plasma sprayed samples under the effect of thermal loads.

In this paper, we present the physical characteristics of the coating of tungsten on graphite using the pulsed laser deposition (PLD) technique. This method was used by different authors for a variety of applications related to fusion. Mostako et al. [20] used PLD to coat tungsten thin films on stainless steel for far-infrared mirrors. The reflectivity obtained is about 91% decreasing by only 2% after submitting the films to an energetic ion beam [21,22]. On the other hand, polycrystalline tungsten targets were coated with W thin films by PLD up to 1 µm thickness [23]. When exposed to high-flux deuterium plasmas, an increase of deuterium retention is observed with decreasing tungsten density and crystallite size and at the same time micro-blisters were observed in the films [24]. Ogorodnikova et al. [25] compare D retention in W coatings produced by three different deposition techniques, including the PLD, on different substrates. The disordered W coated by PLD has the highest D concentration. Moreover, they show that deposition parameters, such as gas pressure, argon ion implantation, temperature of substrate, and deposition rate, affect the crystallite size, therefore the D retention in the coating. Lasers of the PLD were also used to clean mirrors in order to remove the layers of contaminants sputtered from a tokamak that reduces significantly the reflectivity [26] as well as to simulate thermal effects on nanostructures tungsten-based materials [27]. In order to simulate the deposition processes, W-O coatings were loaded with He by implanting He^+ ions on W films grown by pulsed laser deposition (PLD). Appropriate experimental parameters generated porous as well as compact W structures, which greatly affects the He retention [28].

We use different diagnostics to investigate the different aspects of the coating as we change the laser energy. In the next section, we discuss the PLD coating technique and a brief discussion of the substrate used for the deposition. This is followed by estimating the coating thickness using the Rutherford backscattering technique. The results from the scanning electron microscope (SEM) are discussed in Section 4 where we show that the coating is rather uniform. Using the energy dispersive X-ray spectrometry in Section 4.2, we found that the level of impurities remain quite low about 1% while putting forward the change in the profile shape when high laser energies are used. With the X-Ray Diffractometry (XRD) technique (Section 5), we show that the tungsten coating takes place in the form of a body-centered cubic (BCC) crystal that comes on top of the hexagonal graphite. We show that the crystallite size increases with the laser energy and deposition time, whereas the stress decreases and then remain unchanged for a laser energy above 500 mJ.

Fig. 1. A picture of the PLD vacuum chamber where one can see the target and the place we install the substrate. The laser comes at an incident angle about 45°. The target rotates during deposition so the laser interacts with different positions. The temperature of the substrate is set to 500 °C.

2. The pulsed laser deposition setup

The pulsed laser deposition (PLD) technique uses a high-energy pulsed laser to ablate a material [29,30] that performs the coating on a target installed few centimeters away from the impact. The state of the target changes from solid to liquid and then to gas and finally to plasma, which expand either in vacuum or in an ambient gas. The main advantage of this technique is that the coating takes place under high vacuum conditions, hence reducing the presence of impurities in the coated sample. Moreover, one can coat almost any type of material since the laser energy can be chosen to be high enough to at least evaporate parts of the target.

A picture of inside the PLD vacuum chamber is provided in Fig. 1, where the target and the substrate holders are installed. The laser is incident on the target with an angle of 45° and this is illustrated by a triangle. The chamber back pressure is 1.3×10^{-4} Pa obtained using a turbo and a diaphragm pump but the introduction of an Argon gas through a mass flow controller brings it up to 2 Pa during the coatings. At this level, the mean free path of neutral argon is several centimeters, hence, it does not affect the coating process but will leave the quartz window from which the laser penetrates clean from being coated by tungsten.

The krypton-fluoride (KrF) excimer laser emits at the wavelength λ_L = 248 nm with energy up to 600 mJ, the pulse duration is 20 ns and the repetition rate used here is 20 Hz. The beam is focused on a spot size of 2.5 mm^2 leading to a fluence of about 20 J/cm^2. The total time of the coating is set to 4 h except when stated otherwise. The target is mounted on a rotating circular drive so that the incident laser would cover the whole surface of the target ensuring a homogeneous evaporation of the surface layer. The substrate to be coated is installed at a distance of 5 cm from the target. The substrate holder is equipped with a heater that enables us to control its temperature during deposition. It is set to 500 °C after a transient heating to 800° for 1 h to remove the gases that could be trapped on the substrate surface.

2.1. The graphite sample

The substrate used in this study is the Sigrafine R6710 graphite

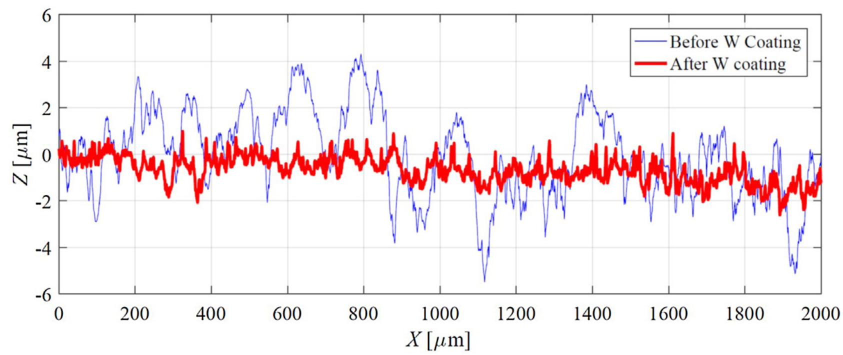

Fig. 2. Two depth profiles as a function of distance are plotted one taken before the tungsten deposition and the other after. The deposition conditions are PLD laser energy 450 mJ, pulse frequency 20 Hz, duration of the coating 4 h, background Argon pressure 2 Pa. The surface clearly is smoother after the coating.

(SGL) with a thickness of 5 mm and a diameter about 2 cm, a type of graphite used at ASDEX-Upgrade for W coatings. The main reason behind using this type of graphite is its thermal expansion, which is proposed to minimize the cracks after being subject to a high heat load as explained by Neu et al. [6]. The substrates are porous and were used without surface treatment other than just out-gazing by heating them up to 800° before bringing the temperature down to 500° at which the tungsten coating is performed. We assess the roughness of our substrate by using a surface profilometer, which measures the depth variation of the sample as a function of position. The plot in Fig. 2 shows two graphs representing the depth as a function of distance before and after the tungsten coating. The standard deviation of the signal yields an estimate of the roughness reaching 1.6 μm in excellent agreement with the grain size estimate supplied by the manufacturer that is about 3 μm. After the tungsten coating, the surface becomes clearly smoother with much less depth variations.

3. Tungsten layer thickness measurement using the RBS

The Rutherford backscattering spectrometry (RBS) technique is used to determine the thickness of the tungsten layers that result from the PLD deposition of W on C. Recently, it was used to assess the different types of tungsten coatings under different experimental parameters [28]. It remains one of the best nondestructive and absolute methods used to determine the thickness, the composition, and to reproduce the elemental depth profile of sub-micron metal layers as discussed by Wang and Nastasi [31] and Roumié et al. [32]. The 5SDH Pelletron Tandem accelerator of 1.7 MV, located at the Lebanese Atomic Energy Commission (see [33]), is used to perform the analysis on samples placed normal to the incident 2 MeV α-particles beam. A partially depleted Passivated Implanted Planar Silicon (PIPS) detector from Canberra, with 14 keV of energy resolution and 25 mm^2 of active area, detects the backscattered particles at a scattering angle of 165° with respect to the incident beam direction. The ion beam energy is calibrated using standard samples consisting of thin layers of gold on silicon and chromium on silicon oxide, and by using the $^{16}O(\alpha,\alpha)$ resonance at 3.034 MeV. The RBS spectra were processed using SIMNRA (6.06 version) program simulation code (Mayer, SIMNRA User's guide [34]).

Fig. 3(a) shows different RBS spectra, where each spectrum corresponds to a particular sample performed at a given PLD laser energy E_L (from 300 to 600 mJ). The most energetic particles are those coming from the top surface, then, the more particles penetrate the more they lose energy due to the beam interaction with the ambient material. The tail in the low energy of the W signal could indicate the roughness of the C substrate or/and a possible diffusion of W into C. This leads to interface layers containing both W and C between the W layer (around 1800 keV) and the C substrate (around 500 keV) with different thicknesses and stoichiometry. The tungsten layer thickness, denoted by $D_{1/2}$, is assessed by layers containing 90% of W. It is plotted as a function of the laser energy in Fig. 3(b).

As a function of the laser energy, a net increase in the coating layer thickness is observed at laser energies above 500 mJ. Below this value, we record thicknesses about 150 nm, whereas for $E_L > 500$ mJ, $D_{1/2}$ jumps to 300 nm. The thickness determined using the RBS is in agreement with the one measured using the SEM as it will be shown hereafter. This makes the coating rate about 1.25 nm/min smaller from those encountered when coating on Rh, W or Cu, which score values respectively about 4, 6 and 8 nm/min [35].

4. Coating properties using the SEM

The coated sample is studied using the MIRA3 TESCAN Scanning Electron Microscope (SEM) with the goal to characterize the surface morphology. For the sample analyzed here, the PLD laser energy is 500 mJ and the ambient argon pressure is set to 2 Pa as the coating took place over a period of 4 h at a pulse frequency of 20 Hz. In Fig. 4, we show images of the coated graphite sample at different magnifications. In (a) the whole sample is shown where the W-coated region is the light gray disk that one can see on top of the darker gray graphite substrate; the disk shape is caused by the target holder. From this picture, we deduce that a rather uniform coating is achieved throughout the exposed area. In (b) and (c), we use a higher magnification in order to highlight the fact that the tungsten penetrates the graphite roughness structures and the coating does not present cracks nor holes. The coating ‘structure’ reflect that of the substrate for example when stainless steel is used a much more uniform coating was obtained [20] and our results appear similar to porous-W obtained earlier in Mateus et al. [28].

4.1. The interface layer

In order to study the interface between the tungsten and the graphite, we perform a cut in the sample and place it vertically, in a special holder, to be imaged by the SEM. We use 10 kV as the electron beam acceleration voltage, the working distance is 12 mm, and the magnification is set at 42,000. In Fig. 5, two images of the same area are shown, where in (a) we use the SE (Secondary Electron Detector), whereas the image using BSE (Back Scattered Electron detector) is shown in (b). Clearly, on the SE image (in (a)), we are not able to obtain a conclusive difference between the deposition and the substrate. The BSE image (in (b)) allowed us to identify the deposited layer, since it is more sensitive than the SE to the variation of the atomic number Z. One may deduce an estimate of the coated thickness to be 300 nm in agreement with the RBS estimate.

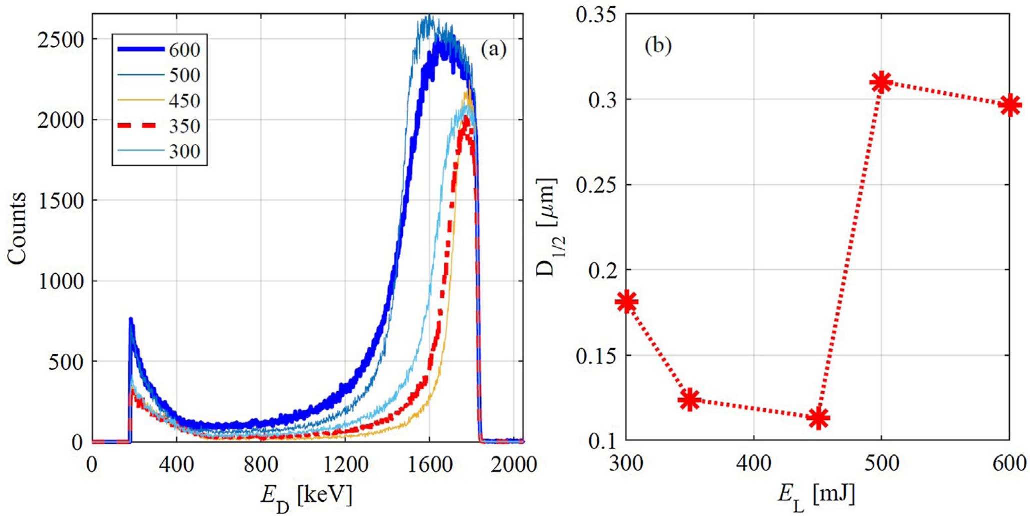

Fig. 3. (a) RBS spectra of the studied samples showing the yields of α particles (counts) as function of their backscattered energies detected by the PIPS detector for different PLD laser energies. The samples were coated with at a total duration of 4 h at 20 Hz repetition rate and an ambient argon pressure of 2 Pa. In (b), we plot the dependence of the tungsten layer thickness on E_L.

4.2. Coating properties using the EDX

We analyze the surface structure using the Energy Dispersive X-ray Spectrometry (EDX) from Oxford Scientific XMAX20, which makes use of the X-ray spectrum emitted by the solid sample bombarded with the SEM beam of electrons to obtain a local analysis of the constituent materials. In Fig. 6(a), we zoom on the region between the W-coated and the graphite regions using the SE detector where a visual inspection of the two regions allows us to deduce that the roughness of the surface area is reduced. This can be quantified using the surface Profilometer where the standard deviation increases from 1.6 up to 5 μm when the sample is coated with 500 mJ laser energy. In Fig. 6(b) we show an EDX image where the colors reflect the three components of the surface layer: tungsten in blue, carbon in red and oxygen in green. It is verified that only these three atoms are detected in our sample. In Fig. 6(c), we show the X-ray intensity as a function of wavelength, plotted in keV for an electron beam accelerated to 12 kV. We thus identify the lines in the spectrum, a task straightforward owing to the simplicity of X-ray spectra. One may thus deduce the tungsten contribution as well as estimate the oxygen impurity concentration in the sample.

The concentration of the different elements as a function of depth in the coating entails measuring the line intensities for each element in the sample and plotting the result as a function of the electron beam energy (E_b), which is proportional to depth. The result yields the weight percentages of tungsten and oxygen and is shown in Fig. 7 for different PLD incident laser energies scanning from 300 to 600 mJ.

With increasing PLD laser energy, we note two effects: (1), the percentage of the coated region by tungsten increases from about 87 to 95%. Moreover, if we assume that the decay has an exponential shape of the form $\exp(-E_b/\lambda_E)$, the λ_E increases with E_L going from $\lambda_E \simeq 6$ kV for $E_L < 500$ mJ to about $\lambda_E \approx 15$ kV for $E_L \geq 500$ mJ. One interpretation is that for low laser energies, and thus a lower coating rate, the tungsten coating follows the shape of the graphite surface. Therefore, for low E_L, the decay with depth reflects mainly the roughness of the sample. For higher E_L, thus higher coating rates, the tungsten starts to fill the gaps of the graphite sample, hence increasing significantly the decay length of the electron probing beam.

The concentration of impurities in these layers are of importance for fusion application and for the quality of the interface layer. Using the same set of data, Fig. 7(b) shows the concentration of oxygen as a function of the electron beam voltage. No clear dependence on E_b is detected indicating that the 1% is the residual oxygen levels in the ambient gas as well as inside the graphite samples before coating. The low oxygen concentration is in agreement with previous PLD coating of tungsten where the impurity presence was shown to increase with the background pressure [23].

5. The W coating structural properties using the XRD

The X-ray diffraction (XRD) technique allows us to gain information about the structural properties of the coating. We use the grazing incident XRD, also called GIXRD, to do our measurements on a XRD D8

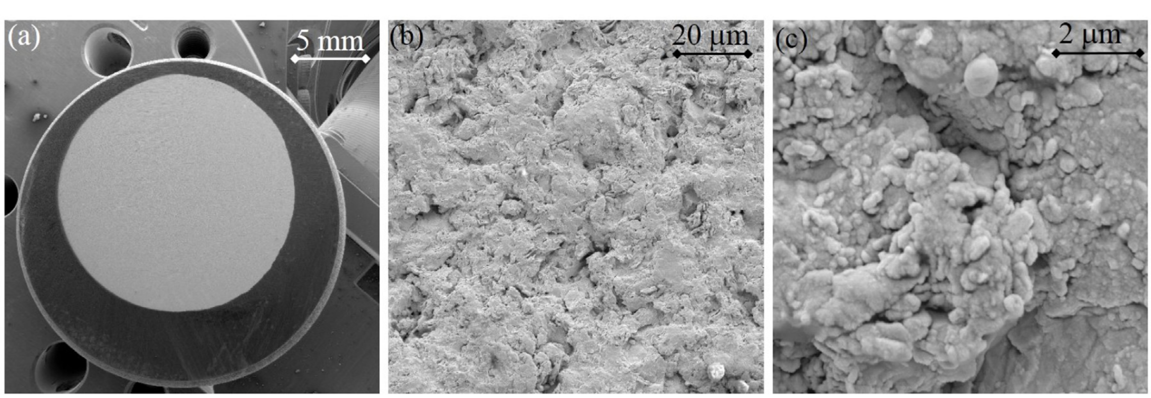

Fig. 4. We use a 10 kV electron beam to generate the three SEM pictures. In (a), the magnification is set to 5 to image the whole sample with the tungsten coating that causes the bright disk on top of the darker graphite disk. In (b), the magnification is set to 1280 allowing us to zoom on the tungsten region to show that the coating is rather uniform across the sample with no appearance of cracks. This is further verified in (c) with a magnification set to 15,300 where we zoom even more on the tungsten-coated region showing a fully covered sample.

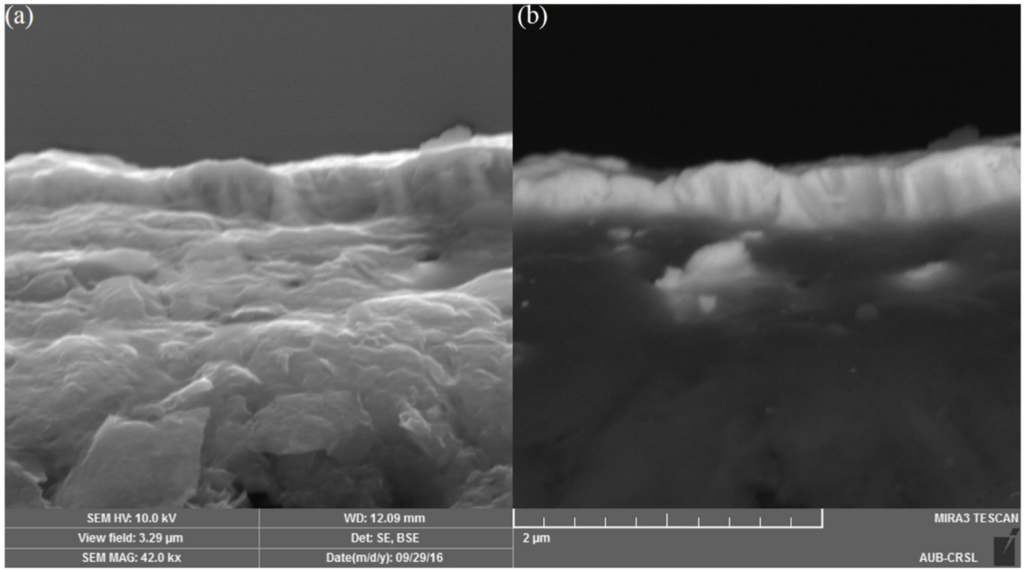

Fig. 5. In (a) and (b), we show two SEM images using the SE and BSE detectors respectively of a W-coated sample that was cut and presented vertically to the electron beam. Using the BSE, the tungsten coating appears in bright gray whereas the graphite substrate in dark gray.

DISCOVER device from Bruker. The X-ray tube emits electromagnetic waves directed at grazing incidence with respect to the sample surface and a rotating X-ray detector measures the diffracted light intensity as a function of the angle 2θ. The diffraction pattern of a sample is reflected by various peaks each corresponding to a different phase. The XRD allows the determination of the average spacing among the layers of atoms, the orientation of the constituent crystals or grains, stress evaluation in specific regions and the crystalline structure of the different materials composing the sample.

5.1. *The crystal structure*

The samples are coated using the PLD for 4 h at a frequency of 20 Hz, except the sample at 400 mJ where this duration is extended to 6 h.

Fig. 8 shows the XRD spectra for the different PLD laser energies as a function of 2θ without modification of the background. The black curve is that of the graphite substrate obtained in the absence of the tungsten coating. It shows peaks at about 42.4, 44.4, 54.4 and 77.5° indicating a pattern found in hexagonal disordered graphite as shown by Li et al. [36] and Zhou et al. [37].

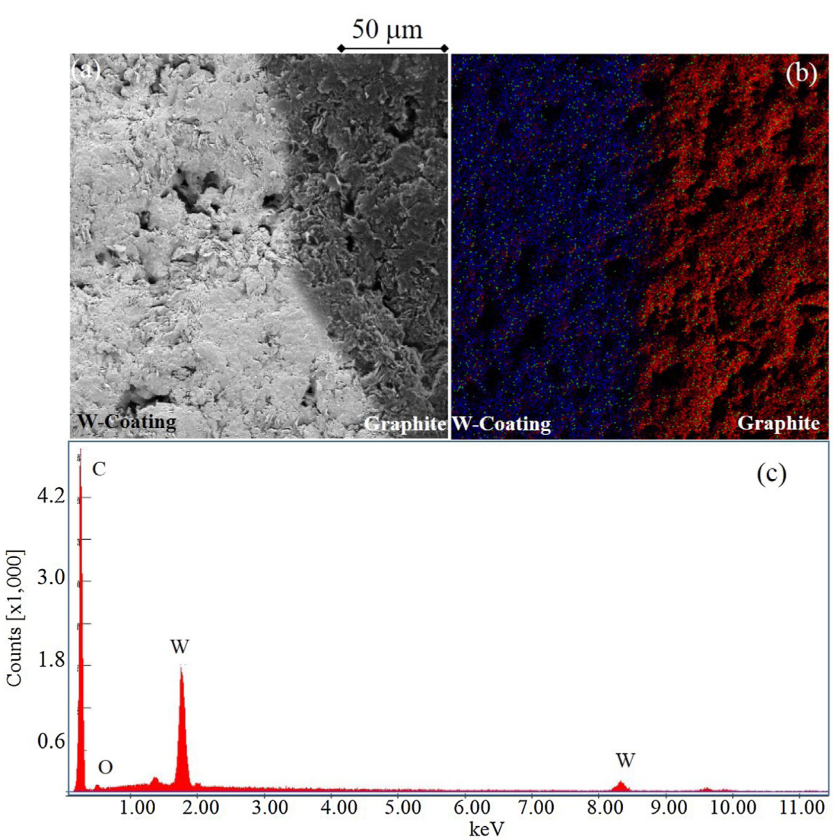

Fig. 6. In (a), a SEM image of the region that is at the interface between the coated and the uncoated area using the SE detector. In (b), we show the same but using the EDS signal where tungsten is shown in blue, carbon is in red and oxygen in green. A typical EDS spectrum is plotted in (c) where the photon counts are plotted as a function of the electrons energy in keV.

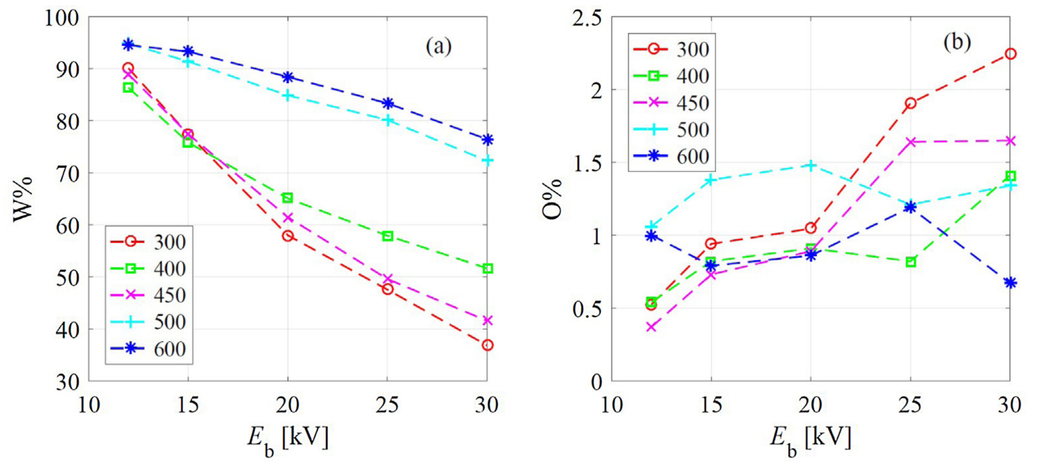

Fig. 7. In (a), we plot the tungsten composition as a function of the electron energy showing the tungsten coating decreasing as we probe deeper into the sample. This is done for different laser energies ranging from 300 to 600 mJ. In (b), we show the results obtained for the oxygen impurity.

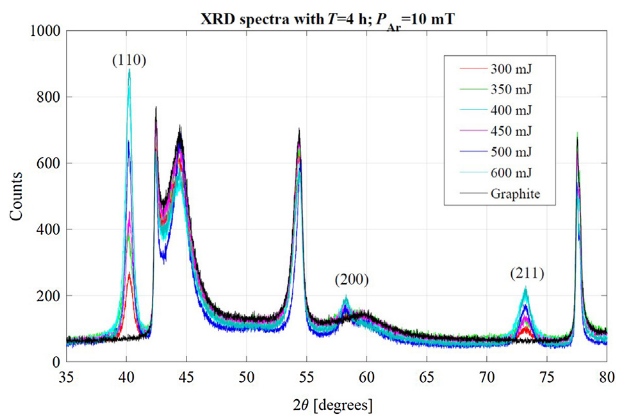

Fig. 8. The photon counts is plotted as a function of the detector angle XRD spectra for graphite as well as for the tungsten coated samples using different PLD laser energies. The spectrum taken with E_L = 400 mJ.

With the tungsten coating, three new peaks appear around 40.3, 58.3 and 73.2° corresponding to the crystalline formation in the (110), (200) and (211) directions. Our first conclusion is that the tungsten coating is done according to a crystalline structure. Moreover, since the sum of each peak is even, it indicates a body-centered-cubic (BCC) structure that is on top the hexagonal structure of the graphite substrate. From the position of the XRD peaks and the atomic radius of tungsten, one can show that indeed the three peaks respectively correspond to ($h = 1$, $k = 1$, $l = 0$), ($h = 2$, $k = 0$, $l = 0$) and ($h = 2$, $k = 1$, $l = 1$). Moreover, we assess the unit cell dimension for the tungsten layer to be 0.317 nm, that is greater than that of the substrate equals to 0.246 nm. The (110) and (211) peaks caused by the tungsten layer are well above the noise and we record no presence of graphite peaks that pollute their shape. This is not the case for the (200) peak, where a number of peaks in this regions are recorded for pure graphite as shown by Li et al. [36,38], which modify the shape of the peak caused by the tungsten. Consequently, we use the (110) and (211) to determine the structural properties of the coating and their dependence on the laser energy. We note that similar XRD spectra, hence similar crystal structure, were obtained in Ogorodnikova et al. [25] using standard vacuum magnetron-sputtering on isotropic fine grain graphite without argon ion implantation.

5.2. Strain causing spectra shift

In Fig. 9(a) and (b), we plot a zoom around the 2θ = 40 and 73° respectively. The angles corresponding to the maxima of the peaks at (110) are shifted toward lower values when compared to the theoretical value of 40 . 3°. This indicates that the tungsten lattice is in the state of strain. In Fig. 8(c), we plot the variation of the lattice strain, defined as $\epsilon = \Delta D/D = (D_{exp} - D_{ref})/D_{ref}$, as a function of the laser energy. The strain-free inter-planer spacing reported in the reference data is D_{ref}, whereas, D_{exp} is the experimentally observed inter-planer spacing of the tungsten film. The positive values of $\Delta D/D$ reflects the tensile nature of the lattice. In (d), we show the amplitude of the two peaks showing a net increase with E_L, which reflects an increase in the coated layer. It is increases 5 folds where E_L is multiplied by a factor of 2.

5.3. Crystallite size of the tungsten film

We turn now to analyze the broadening of the spectra caused by the effects of the strain as well as the crystallite size. Both of these mechanisms contribute up to a certain degree to the observed broadening of the spectra. The first is caused by the finite size of the mono-crystals and the second by the change in the lattice dimensions as the BCC tungsten is deposited on top of the hexagonal graphite structure.

We verified that fitting the experimental curve by a Voigt or a pseudo-Voigt profile leads similar results and accurately reproduce the experimental profiles. The Voigt profile results from the convolution of a Gaussian and a Cauchy (Lorentzian) profile,

$$V(\theta) = \int G(\theta')L(\theta - \theta')d\theta'$$

where

$$G(\theta) \sim \exp - (\theta - \theta_0)^2/2\sigma_G^2 \quad \text{and} \quad L(\theta) \sim 1/((\theta - \theta_0)^2 + \sigma_L^2/4),$$

whereas the Pseudo-Voigt profile is a linear addition of the two

$$\mathrm{PV}(\theta) = \nu G(\theta) + (1 - \nu)L(\theta).$$

From the pseudo-Voigt fit, we verify that the Gaussian distribution dominates the experimental fit with $\nu \approx 0.7$ for all the samples and at the different laser energies. Consequently, in order to assess the contribution of the strain and the crystallite size on the broadening of the spectra, we use the Williamson-Hall (WH) plot where the integral breadth of the experimental curve, denoted by β, is the sum of the squares of the strain and the crystallite size:

$$(\beta\cos\theta_0)^2 = \left(\frac{K\lambda}{A}\right)^2 + (4\epsilon\sin\theta_0)^2. \tag{1}$$

The values of crystallite size, A, and the strain, ϵ, are obtained using the two peaks (110) and (211) and the result is plotted in Fig. 10(a) and (b) respectively. The crystallite size increases from 30 to 50 nm as the

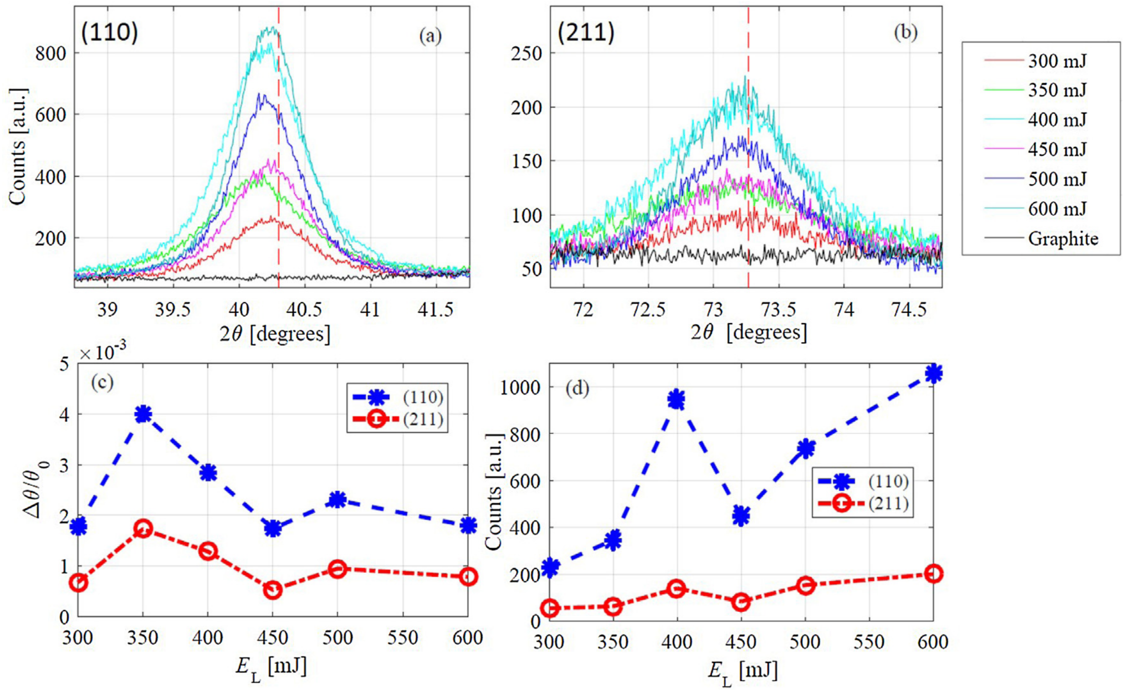

Fig. 9. In (a) and (b) we zoom on the XRD spectra with the tungsten coating obtained with different laser energies around $2\theta \approx 40^{\circ}$ and $2\theta \approx 73^{\circ}$ respectively. In (c), we assess the micro-strain from the shift of the spectra toward lower angles when compared with the no-stress cases that is illustrated in the dashed vertical lines in (a) and (b). In (d), we plot the amplitude of the peaks as a function of the laser energy.

laser energy goes from 300 to 600 mJ. Note the sample at 400 mJ, which is coated for 6 h, presents a crystallite size of about 85 nm, much greater than the interpolated one using the 4-h data estimated to be about 35 nm. Using the Scherrer formula, we have another estimate of the crystallite size as

$$A_S = \frac{K_s \lambda}{\beta \cos\theta_0}, \tag{2}$$

where the Scherrer constant is $K_s = 0.94$. As it can be deduced from Fig. 9(a), the effect of the coating time is not detected for either of the two peaks since the latter assumes that all the broadening is caused by the crystals size and this leads to underestimating the values of A. It was found that the crystallite size depends on the background pressure, as higher Helium background pressure lead to more amorphous films as shown in Dellasega et al. [23].

5.4. The micro-strain of the tungsten film

Using Eq. (1), we determine the micro-strain of the tungsten coating. The result is plotted in Fig. 10(b) where the values increase from 1.9×10^{-3} to 3.6×10^{-3} at first for laser energies increasing from 300 to 400 mJ. Then, it decreases to 2.5×10^{-3} to become independent of E_L. The values as well as the dependence on E_L are in good agreement with ϵ estimated from the angular shift of the peaks. They all indicate that the tungsten coating has a positive strain indicating tensile stresses and that it appears to become independent of the laser energy

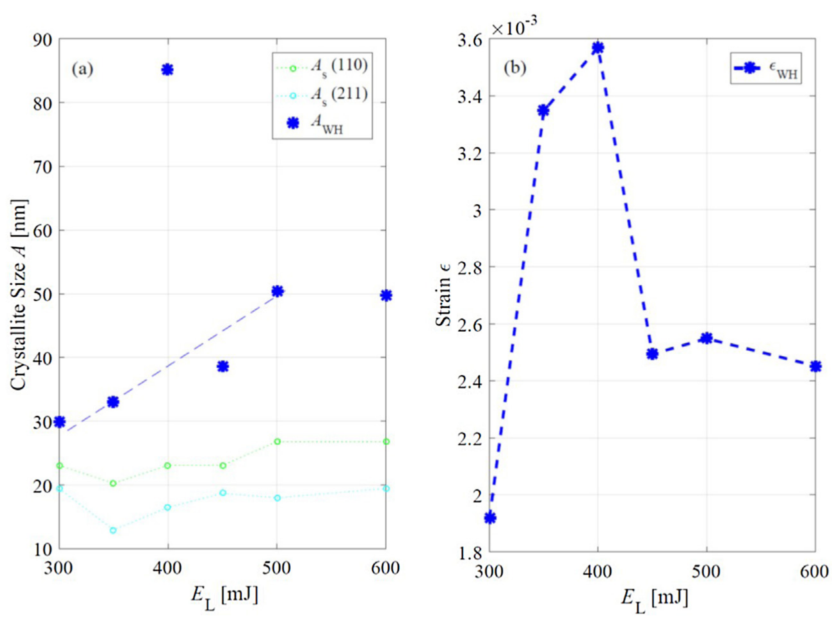

Fig. 10. In (a), we plot the tungsten crystallite size estimated using different methods as a function of E_L. We use '★' for data analyzed with the Williamson-Hall method which separates the contributions of the strain from that of the crystal size using information from the two peaks at (110) and (211). in '∘' the crystal size as obtained using the Scherrer formula where the width of the XRD spectra is assumed to be solely caused by the finite crystallite size. In (b), we show the strain as obtained using the WH method (in ★).

for $E_L \geq 500$ mJ.

6. Conclusion

In this paper, we study the properties of tungsten coating on graphite obtained using the pulsed laser deposition technique used to our best knowledge for the first time for fusion applications. The sample used is fine grain graphite, which is amorphous with a grain size of about 3 µm. As a parameter of coating, we use the laser energy, which can be changed while keeping the repetition rate, the argon background pressure, the substrate temperature and the total time of coating constant. The coating obtained is characterized using different techniques each giving a specific information. Using the SEM imaging, we verified that the coating obtained is rather uniform and that there are no visible cracks nor voids. The impurity level, namely that of oxygen, is shown to remain limited to low levels about 1%. Using the XRD, we were able to show that (1) the graphite substrate has an hexagonal structure and that (2) the tungsten coating has a BCC crystal form. The strain that results from the difference in the crystal type and size is measured to be about 2×10^{-3} using the shift and the broadening of the spectra. We were also able to determine the crystallite size and show that it increases with laser energy from 20 to 50 nm. The laser energy increase leads to an increase in the tungsten thickness going from 120 to 300 nm as measured using the RBS, which also indicated, in agreement with other diagnostics that the coating properties are different for PLD laser energy above and below 500 mJ. From this study, it appears using laser energy of 500 mJ yield the best coating.

Future work will be focused on submitting these samples to a high heat load of the order of 10 MW/m^2 using the same laser but with attenuated energy. The reason is to try to understand the effects high heat loads such the ones produced by ELMs on these coatings. We thus aim at linking the properties of the coating presented in this paper to their behavior under high heat loads.

Acknowledgements

This work is funded by the University Research Board (grant 103186), by the Kamal A. Shair CRSL Research Fund (grant 103191) at the American University of Beirut as well as by the Lebanese Counsel for Scientific Research (grant 522317).

References

[1] E. Hinnov, K. Bol, D. Dimock, R. Hawryluk, D. Johnson, M. Mattioli, E. Meservey, S. Von Goeler, Effects of tungsten radiation on the behaviour of PLT tokamak discharges, Nucl. Fusion 18 (1978) 1305.
[2] G. Sergienko, B. Bazylev, T. Hirai, A. Huber, A. Kreter, P. Mertens, A. Nedospasov, V. Philipps, A. Pospieszczyk, M. Rubel, et al., Experience with bulk tungsten test-limiters under high heat loads: melting and melt layer propagation, Phys. Scr. 2007 (2007) 81.
[3] K. Krieger, H. Maier, R. Neu, A.U. Team, Conclusions about the use of tungsten in the divertor of ASDEX Upgrade, J. Nucl. Mater. 266 (1999) 207–216.
[4] M. Mayer, V. Rohde, G. Ramos, E. Vainonen-Ahlgren, J. Likonen, J. Chen, Erosion of tungsten and carbon markers in the outer divertor of ASDEX-Upgrade, Phys. Scr. 2007 (2007) 106.
[5] A. Herrmann, H. Greuner, J. Fuchs, P. De Marné, R. Neu, A.U. Team, Experiences with tungsten coatings in high heat flux tests and under plasma load in ASDEX Upgrade, Phys. Scr. 2009 (2009) 014059.
[6] R. Neu, H. Maier, E. Gauthier, H. Greuner, T. Hirai, C. Hopf, J. Likonen, G. Maddaluno, G. Matthews, R. Mitteau, et al., Investigation of tungsten coatings on graphite and CFC, Phys. Scr. 2007 (2007) 150.
[7] G. Federici, P. Andrew, P. Barabaschi, J. Brooks, R. Doerner, A. Geier, A. Herrmann, G. Janeschitz, K. Krieger, A. Kukushkin, et al., Key ITER plasma edge and plasma-material interaction issues, J. Nucl. Mater. 313 (2003) 11–22.
[8] V. Philipps, Tungsten as material for plasma-facing components in fusion devices, J. Nucl. Mater. 415 (2011) S2–S9.
[9] R. Doerner, The implications of mixed-material plasma-facing surfaces in ITER, J. Nucl. Mater. 363 (2007) 32–40.
[10] H. Maier, J. Luthin, M. Balden, J. Linke, F. Koch, H. Bolt, Properties of tungsten coatings deposited onto fine grain graphite by different methods, Surf. Coat. Technol. 142 (2001) 733–737.
[11] H. Maier, R. Neu, H. Greuner, B. B“oswirth, M. Balden, S. Lindig, G. Matthews, M. Rasinski, P. Wienhold, A. Wiltner, Qualification of tungsten coatings on plasma-facing components for jet, Phys. Scr. 2009 (2009) 014031.
[12] A. Cambe, E. Gauthier, J. Layet, S. Bentivegna, Development of tungsten coating for fusion applications, Fusion Eng. Des. 56 (2001) 331–336.
[13] X. Liu, F. Zhang, S. Tao, Y. Cao, Z. Xu, Y. Liu, N. Noda, Research and development of plasma sprayed tungsten coating on graphite and copper substrates, J. Nucl. Mater. 363 (2007) 1299–1303.
[14] H. Maier, R. Neu, H. Greuner, C. Hopf, G. Matthews, G. Piazza, T. Hirai, G. Counsell, X. Courtois, R. Mitteau, et al., Tungsten coatings for the jet ITER-like wall project, J. Nucl. Mater. 363 (2007) 1246–1250.
[15] C. Ruset, E. Grigore, I. Munteanu, H. Maier, H. Greuner, C. Hopf, V. Phylipps, G. Matthews, J.E. Contributors, et al., Industrial scale 10 µm W coating of CFC tiles for ITER-like wall project at jet, Fusion Eng. Des. 84 (2009) 1662–1665.
[16] H. Maier, M. Rasinski, E. Grigore, C. Ruset, H. Greuner, B. B”oswirth, G. Matthews, M. Balden, S. Lindig, et al., Performance of W coatings on CFC with respect to carbide formation, J. Nucl. Mater. 415 (2011) S310–S312.
[17] C. Ruset, E. Grigore, H. Maier, R. Neu, H. Greuner, M. Mayer, G. Matthews, Development of W coatings for fusion applications, Fusion Eng. Des. 86 (2011) 1677–1680.
[18] C. Ruset, E. Grigore, D. Falie, M. Gherendi, H. Maier, M. Rasinski, G. Matthews, V. Zoita, J. EFDA, The impact of thermal fatigue and carbidization on the W coatings deposited on cfc tiles for the ITER-like wall project at jet, Fusion Eng. Des. 88 (2013) 1690–1693.
[19] H. Kim, H.J. Lee, S.H. Kim, C. Jang, Plasma thermal performance of a dual-process PVD/PS tungsten coating on carbon-based panels for nuclear fusion application, Fusion Eng. Des. 109 (2016) 590–595.
[20] A. Mostako, C. Rao, A. Khare, Mirrorlike pulsed laser deposited tungsten thin film, Rev. Sci. Instrum. 82 (2011) 013101.
[21] A. Mostako, A. Khare, C. Rao, P.M. Raole, S. Vala, S. Jakhar, T. Basu, M. Abhangi, R.J. Makwana, Effect of hydrogen ion beam irradiation onto the FIR reflectivity of pulsed laser deposited mirror like tungsten films, J. Nucl. Mater. 423 (2012) 53–60.
[22] A. Mostako, A. Khare, C. Rao, S. Vala, R. Makwana, T. Basu, Deuterium ion beam irradiation onto the pulsed laser deposited tungsten thin films, J. Vac. Sci. Technol. A: Vac. Surf. Films 31 (2013) 061510.
[23] D. Dellasega, G. Merlo, C. Conti, C.E. Bottani, M. Passoni, Nanostructured and amorphous-like tungsten films grown by pulsed laser deposition, J. Appl. Phys. 112 (2012) 084328.
[24] D. Dellasega, A. Pezzoli, M. Passoni, A. Kleyn, P.Z. Van Emmichoven, et al., Deuterium retention and surface modifications of nanocrystalline tungsten films exposed to high-flux plasma, J. Nucl. Mater. 463 (2015) 989–992.
[25] O. Ogorodnikova, J. Roth, M. Mayer, Deuterium retention in tungsten in dependence of the surface conditions, J. Nucl. Mater. 313 (2003) 469–477.
[26] A. Maffini, A. Uccello, D. Dellasega, M. Passoni, Laser cleaning of diagnostic mirrors from tungsten-oxygen tokamak-like contaminants, Nucl. Fusion 56 (2016) 086008.
[27] E. Besozzi, A. Maffini, D. Dellasega, V. Russo, A. Facibeni, A. Pazzaglia, M. Beghi, M. Passoni, Nanosecond laser pulses for mimicking thermal effects on nanostructured tungsten-based materials, Nucl. Fusion 58 (2018) 036019.
[28] R. Mateus, D. Dellasega, M. Passoni, Z. Siketić, I.B. Radović, A. Hakola, E. Alves, Helium load on WO coatings grown by pulsed laser deposition, Surf. Coat. Technol. 355 (2018) 215–221.
[29] G.K. Hubler, Pulsed laser deposition, MRS Bull. 17 (1992) 26–29.
[30] M. Stafe, C. Negutu, N.N. Puscas, I. Popescu, Pulsed laser ablation of solids, Rom. Rep. Phys. 62 (2010) 758–770.
[31] Y. Wang, M.A. Nastasi, Handbook of Modern Ion Beam Materials Analysis, Materials Research Society, Warrendale, Pennsylvania, 2009.
[32] M. Roumié, F. Lmai, A. Awada, K. Zahraman, B. Nsouli, A. Zaiour, M. Hage-Ali, M. Ayoub, J. Faerber, Depth profiling and stoichiometry of constituents in platinum electroless contacts on CdTe (111) under different pH values, Thin Solid Films 515 (2007) 7843–7846.
[33] M. Roumié, B. Nsouli, K. Zahraman, A. Reslan, First accelerator based ion beam analysis facility in Lebanon: development and applications, Nucl. Instrum. Methods Phys. Res. Sect. B: Beam Interact. Mater. Atoms 219 (2004) 389–393.
[34] M. Mayer, U.G. Simnra, Technical Report IPP 9/113, Max-Planck Institut fur Plasmaphysik, Garching, Germany, 1997 There is no corresponding record for this reference.
[35] A. Mostako, A. Khare, C. Rao, S. Vala, T. Basu, P.M. Raole, R. Makwana, Post-irradiation effect of deuterium ion beam onto Rh/W/Cu multilayer thin film, J. Nucl. Mater. 446 (2014) 63–67.
[36] Z. Li, C. Lu, Z. Xia, Y. Zhou, Z. Luo, X-ray diffraction patterns of graphite and turbostratic carbon, Carbon 45 (2007) 1686–1695.
[37] Z. Zhou, W. Bouwman, H. Schut, C. Pappas, Interpretation of X-ray diffraction patterns of (nuclear) graphite, Carbon 69 (2014) 17–24.
[38] J. Li, X. Liu, C. Cheng, T. Hayat, N.S. Alharbi, A. Alsaedi, X. Wang, Preparation of micron sized graphite using a spark plasma technique, RSC Adv. 6 (2016) 50776–50779.